Research Article Vol. 35, No. 12 / December 2018 / Journal of the Optical Society of America B 3049

Journal of the Optical Society of America B

OPTICAL PHYSICS

Optical focusing based on the planar metasurface reflector with application to trapping cold molecules

WEIYANG CAI,[1] HAIYU YU,[1] SUPENG XU,[1] MENG XIA,[1] TAO LI,[2] YALING YIN,[1] YONG XIA,[1,3,*] AND JIANPING YIN[1]

[1]State Key Laboratory of Precision Spectroscopy, Department of Physics, East China Normal University, Shanghai 200062, China
[2]National Laboratory of Solid State Microstructures, College of Engineering and Applied Sciences, Nanjing University, Nanjing 210093, China
[3]NYU-ECNU Institute of Physics at NYU Shanghai, Shanghai 200062, China
*Corresponding author: yxia@phy.ecnu.edu.cn

Received 10 July 2018; revised 18 October 2018; accepted 24 October 2018; posted 24 October 2018 (Doc. ID 338286); published 15 November 2018

We demonstrate theoretically a 2D subwavelength silicon-grating reflector with strong focusing capability and the potential application to an optical dipole trap of cold molecules such as MgF. We study the dependence of the focusing properties of this reflector on its structural parameters, numerical aperture, and fabrication-error tolerance. Our study shows that the reflector delivers high reflectivity and strong focusing performances with the maximum intensity at the focal point over 200 times the incident one. Such a focusing field on the reflector can provide a deep potential to trap cold MgF molecules from a standard magneto-optical trap.

https://doi.org/10.1364/JOSAB.35.003049

1. INTRODUCTION

Metasurfaces are subwavelength arrays of thin optical elements (either dielectric or metal) [1–3]. By adjusting the geometric parameters of the structural element, such as shape, size, and orientation, we can locally divert the phase of the incident light to control the reflected or transmitted wavefront. So, one can design the structural element to interact with the components of electric and magnetic fields independently to control the polarization, phase, amplitude, and dispersion of the light [4–7]. Due to their versatility and design flexibility as well as straightforward fabrication, metasurface-based optics can potentially replace or complement their conventional refractive and diffractive counterparts. Metasurface-based lenses have attracted considerable attention. For example, Yin *et al.* achieved an in-plane focusing by exciting plasmon interference through a series of holes [8]. In-plane focusing with circular/elliptical slit apertures was also reported by Liu *et al.* [9]. More reports studied that the visible light was focused in the far field by using quasiperiodic arrays of nanoholes [10]. Although significant progress has been made on the plasma surface, the low transmission efficiency at visible and near-infrared wavelengths limits its practical application [11]. These problems can be solved by using dielectric metasurfaces [12,13]. Due to their large index of refraction and sophisticated manufacturing techniques, silicon-based metasurfaces have prospects to realize metalenses, especially in the near-infrared region [14–17]. A 1D amorphous silicon flat focusing grating reflector for which the period and duty ratio of the grating elements gradually change from the center of the lens to the edge has been reported in theory [15] and experiment [16]. A 2D focusing subwavelength grating with high numerical aperture and reflectivity has been studied theoretically, whose focusing ability can be controlled by the period and duty ratio of the grating [18]. Another concave-reflective focusing silicon reflector with varying thickness of the grating has also been proposed [19]. However, due to the high phase dispersion of their building blocks, metasurfaces suffer significantly from large chromatic aberration. Only recently have achromatic metalenses successfully been realized over the visible region and infrared band of 1.2–1.68 μm [20–22].

Our focus in this report is toward surface optical control on the planar metasurface with confined and enhanced fields. Our studies differ from previous work in that we optimize three parameters, the period, duty ratio, and thickness, by which we can get more precise phases. Then we can choose the phase value with high reflectivity and closer to the ideal phase, which can obtain the strong focusing ability. We also consider the impact of a fabrication-error-tolerant design on the focusing performances and discuss the application to trapping cold molecules. It is well known that when an atom (or molecule) moves in an inhomogeneous light field, it will experience an optical dipole force and be attracted toward the maximal optical field. The focusing optical fields form the conservative traps with much smaller trap volumes and controllable trap depths for cold atoms (or molecules), offering nearly state-independent trapping potentials. Such a strong focusing optical field reflected by the metasurfaces can provide a deep potential to trap the cold atoms (or molecules), so it would be interesting and worthwhile to design some controllable optical traps based on the metasurfaces and explore their potential applications in the fields of cold atoms (or molecules). Recently, focusing optical field based on planar diffraction of a grating reflector has been used to achieve magneto-optical trap (MOT) of Rb atoms [23–25].

In this paper, a novel scheme of optical trapping of cold molecules by using a planar metasurface reflector is demonstrated theoretically. We study the properties of the concentric reflective focusing silicon grating on its thickness, period, and duty ratio, and we contrast the focusing properties with different numerical aperture of the reflector. We also study the effect of missing grating strips on the focusing characteristics of the reflector. Finally, we discuss the feasibility of this aperiodic, thickness-variation annular grating reflector serving as an optical dipole trap for MgF molecules.

2. DESIGN AND SIMULATION OF THE PLANAR METASURFACE REFLECTOR

When the light is illuminated at the focusing grating, the reflected light will be converged at the focal point if the phase distribution of the reflected light on the surface of the grating satisfies Eq. (1) [26]:

$$\Phi(x) = \frac{2\pi}{\lambda}\left(\sqrt{x^2 + f^2} - f\right) + \varphi_0, \tag{1}$$

wherein λ is the incident wavelength, f is a given focal length, x is the distance to the center O of the grating, and φ_0 is the reflection phase shift of the grating center O. An aperiodic, thickness-variation concentric-focused grating design process is straightforward. We shall design a 1D reflective focusing grating with variant thickness, period, and duty ratio; then we extend the 1D grating to the corresponding 2D concentric one (the 1D infinitely long grating illuminated by TM polarized light and the 2D concentric grating illuminated by radially polarized light).

The specific procedures are as follows: First, we use the rigorous coupled wave analysis method to determine the reflectivity and reflection phases of a 1D infinitely long grating with varying thickness, period, and duty ratio. Next, according to Eq. (1), we can obtain the phase shift in different positions given the focal length of the focusing grating to be designed. Then, according to the ideal phase shift as a function of different positions, the grating bar with different structure parameters (period Λ, thickness h, and duty ratio η) is chosen to match the phase of the corresponding position (at the same time, the high reflectivity is satisfied). $\Phi(x_n)$ has the form of Eq. (1). The relationship of these parameters can be written as Eq. (2),

According to the design process, we first present an aperiodic, thickness-varyng, and high contrast reflective focusing grating with a focal length of 10 μm under the incident 1550 nm radial polarized light. The grating reflector has a diameter of 44.11 μm, comprising concentric silicon gratings whose refractive index is 3.48 and the silica substrate with a refractive index of 1.54. The cross section of the designed grating reflector is schematically illustrated in Fig. 1(a). Figures 1(c)–1(e) show the relation between the phase shift and the thickness, period, and duty ratio of the grating, respectively. We can find that at the period of 0.676 μm and duty ratio of 0.68, the reflectivity of the grating is more than 80% when the thickness varies from 0.27 to 0.67 μm over the phase shift of $2\pi - 0$ in Fig. 1(c). In Fig. 1(d), at the thickness of 1.2 μm and duty ratio of 0.57, the reflectivity is more than 90% when the period varies from 0.56 to 0.95 μm over the phase shift of 1.88π to -0.6π. Finally, in Fig. 1(e), we can see that at the period of 0.6 μm and thickness of 1.2 μm, the reflectivity is more than 95% when the duty ratio varies from 0.34 to 0.49 over the phase shift of $1.47 - 0.37\pi$. Due to the diversification of the parameters of the grating strip, we can achieve better focusing while maintaining a higher reflectivity by selecting grating strips with more than 90% reflectivity and more accurate phase.

We study the focusing characteristics of this grating reflector, and the results of the simulation are shown in Figs. 1(b) and 1(f). Figure 1(b) shows the field distribution of the cross section on the $x - o - z$ plane. Most of the incident light is reflected, and the overall reflectivity of the grating is ~81.2%. The focal length is about 10.15 μm, close to the designed 10 μm focal length. This is because the phase shift distribution, controlled by this reflector, is discrete rather than continuous. Figure 1(f) shows the 1D relative optical intensity distribution on the cut plane when $z = 10.15$ μm. The light spot has a full-width at half-maximum (FWHM) of 0.85 μm. The maximum optical intensity at the focal point is over 200 times the incident light intensity.

A silicon grating reflector can produce extremely high wideband reflection (or transmission) in the incident direction (or in reverse direction) and ultrahigh quality factor resonances. Here, we first discuss the focusing properties of gratings with different numerical aperture $\mathrm{NA} = \sin(\tan^{-1}(D/2f))$, where D is the width of the reflector and f is the focal length. We design many silicon gratings with the focal length of 10 μm and different numerical aperture according to the approach. At an incident power of 0.5 W for 1550 nm, we study the effect of different numerical aperture on the focusing optical field intensity. The simulation results are shown in Fig. 2. Figure 2(a) shows the reflectivity of different numerical aperture reflectors. We can find that the reflectors have high reflectivity, ranging from 79% to 81.9%. Figure 2(b) shows the relative maximum electric field intensity and the corresponding FWHM at

$$\begin{cases} x_{n+1} = x_n + \frac{1}{2}(\Lambda_n + \Lambda_{n+1}), & n = 0, 1, 2, \ldots \\ \Phi(x_{n+1}) = \Phi(x_n + \frac{1}{2}(\Lambda_n + \Lambda_{n+1})) = \frac{2\pi}{\lambda}(\sqrt{x_{n+1}^2 + f^2} - f) + \varphi_0, & n = 1, 2, \ldots \end{cases}. \tag{2}$$

Finally, the phase of the grating surface is changed from 0 to 2π through the selection of these grating bar parameters.

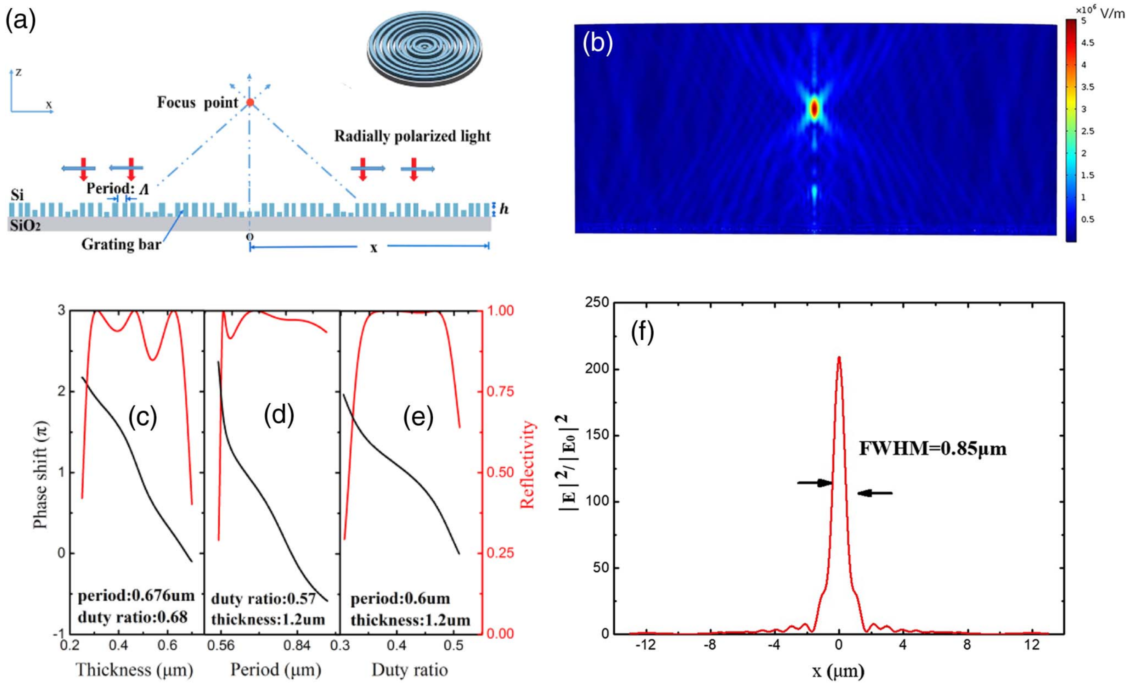

Fig. 1. (a) Structure layout of the concentric circular grating proposed with strong focusing ability. The red arrows represent the incident light direction, and the blue ones show the polarization direction of radially polarized illumination. The inset is the schematic diagram of the circular grating configuration. (b) 2D intensity distribution of the focused beam on the $x - o - z$ plane. (c)–(e) Dependence of the reflectivity (red line) and phase shift (black line) in the reflected plane of 1D infinitely long grating on the (c) grating thickness, (d) period, and (e) width. (f) 1D relative intensity distribution on the x axis at the focusing point $z = 10.15$ μm for panel (b).

different numerical aperture. We can see that as the numerical aperture increases, the optical intensity at the focal point increases first and then decreases. The FWHM gradually declines and eventually remains unchanged. The optical intensity reaches the maximum at the focal point when the numerical aperture is 0.91. This because as the radius of the grating reflector increases, the phase on the grating surface changes more than 2π, which is more conducive to converging light to the focusing point. However, as the reflector numerical aperture further increases more than 0.91, the field intensity gradually reduces. This is because the modulated phase of the grating strip near the edge does not reach an integral multiple of 2π, so the entire reflector deviates from the accurate phase modulation.

We study the focusing characteristics, such as the reflectivity and focal length, of the reflector on the incident wavelength. When the incident wavelength increases, the focal length becomes smaller, from 11 μm at 1490 nm to 7 μm at 1760 nm. The bandwidth $\Delta\lambda/\lambda$ of the reflector at wavelength of 1490–1760 nm is about 17.42%.

For the influence of the missing number of the grating strips on the focusing performance of grating reflectors, at an incident power of 0.5 W, we randomly select the grating strips to make them missing to investigate the corresponding intensity of the

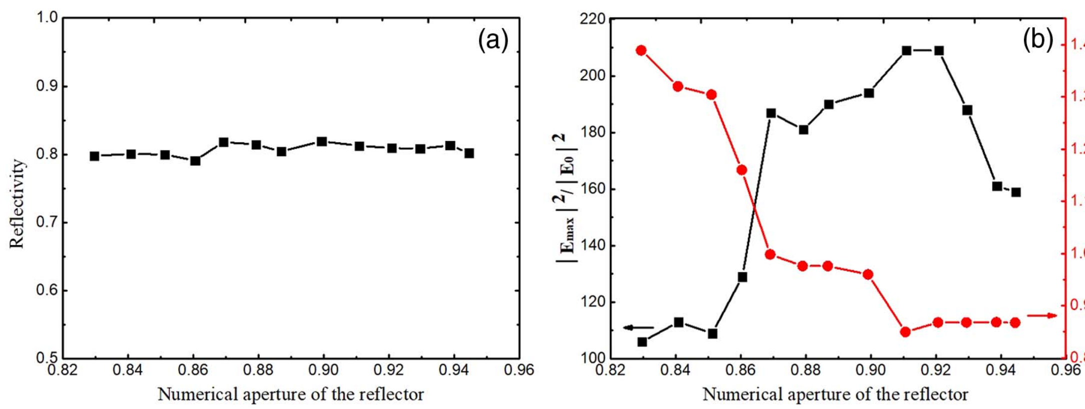

Fig. 2. Focusing properties of the grating reflectors with 10 μm focal length and different numerical aperture. (a) Reflectivity of different NA reflectors. (b) The black line shows the relative maximum optical intensity at different NA, and the red line shows the corresponding FWHM.

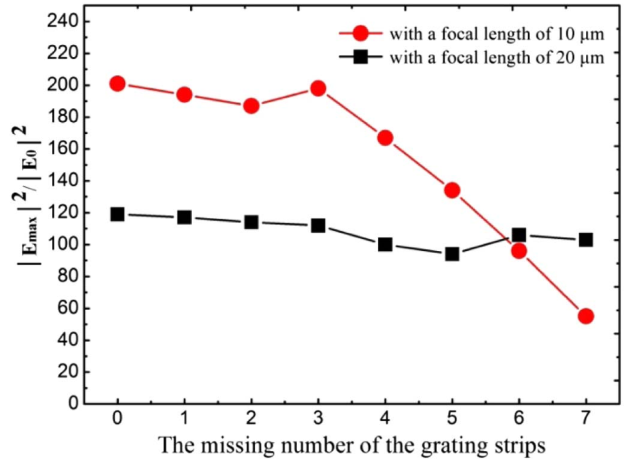

Fig. 3. Influence of the missing number of grating strips on the focusing characteristics of the reflector. The red and black lines depict the relative maximum optical intensity of the reflector with a focal length of 10 μm and 20 μm at the missing of the grating strips, respectively.

focusing point. The theoretical simulation results are shown in Fig. 3. We can see that for a grating reflector with a focal length of 10 μm, the relative maximum field intensity of the focusing point does not change much when a few numbers of the grating strips are absent. However, as the number of the missing grating strips increases, the relative maximum field intensity decreases. For the grating reflector with a focal length of 20 μm, the relative maximum field intensity hardly changes when the number of the missing grating strips increases. Although the grating reflector with 10 μm focal length has larger focused field intensity than the one with a 20 μm focal length, the error of the grating strip has less effect on the 20 μm grating reflector. This is because the diameter of the reflector with 10 μm focal length is much smaller than the one with a focal length of 20 μm, which means the former consists of much fewer numbers of strips than the latter. So, for the former, the missing seven strips have a large effect on their phase modulation.

3. APPLICATION TO TRAPPING COLD MOLECULES

Either atoms or molecules in inhomogeneous fields will be subjected to a dipole effect, and the atoms (molecules) are drawn to the maximum of the light field under the action of this force [27]. This kind of reflective grating with a strong focusing ability provides a deep potential for trapping cold molecules. Here, we discuss the feasibility of this aperiodic, thickness-variation annular grating reflector, which serves as an optical dipole trap.

When a neutral molecule enters into an inhomogeneous light field, it will experience an optical dipole force, which is described by an optical trapping potential [27,28]:

$$\mathrm{U_{dip}} = -\frac{1}{2}\langle pE\rangle = -\frac{1}{2\varepsilon_0 c}\mathrm{Re}(\alpha)I(r), \tag{3}$$

$$F_{\mathrm{dip}}(r) = -\nabla U_{\mathrm{dip}}(r) = \frac{1}{2\varepsilon_0 c}\mathrm{Re}(\alpha)\nabla I(r), \tag{4}$$

wherein α is the molecule polarizability, p is the dipole moment, and $I(r)$ is the optical intensity. The dipole force results from the gradient of the potential, a conservative force, and is proportional to the intensity gradient of the field. When the light field is red detuned, the interaction potential is abstractive, and the molecules will be attracted to the maximum of the light field. Therefore, molecules will be trapped in a red-detuned focusing point. The time averaged force calculated by the stress tensor method and by the dipole force method can lead to the same total force [29–32].

However, due to the further resonance of the laser frequency, caused by the spontaneous scattering of the far red-harmonic laser field, the heating is considered as the main cause of molecule loss in the dipole trap. To quantify the effect, we should ensure the scattering rate. Despite the complexity of the real MgF molecule system, the scattering rate, R, given by the solution to the rate equations is well described over a wide range of intensity and detuning by a function of the same simple form [33],

$$R = \frac{I/(5I_{\mathrm{sat}})}{1 + I/(5I_{\mathrm{sat}}) + 4((\omega - \omega_0)/\Gamma)^2}\frac{1}{10.5}\Gamma. \tag{5}$$

Here, I_{sat} is the saturation intensity, ω_0 is the frequency at resonance, and Γ is the natural linewidth of the dominant transition to the ground state (for MgF molecules, $\Gamma = 2\pi \times 22.2$ MHz [34,35]). Taking MgF molecules as an example, at the incident power of 0.4 W for 1550 nm, we can calculate the optical potential and the dipole force according to Eqs. (3) and (4). We also can calculate the scattering rate according to Eq. (5). The results are shown in Fig. 4. We get the maximum dipole potential for about 1.1 mK, which is high enough to trap cold MgF molecules from a standard MOT with a temperature of 532.7 μK. The corresponding dipole force is $F_{\mathrm{dipole}} = 5.4 \times 10^{-22} N$, which is at least 7500 times the gravity force exerted on an MgF molecule. This shows that the dipole force is strong enough to balance the action of the gravity force on the molecules. In addition, the maximum photon scattering rate of MgF molecule in the optical trap is lower

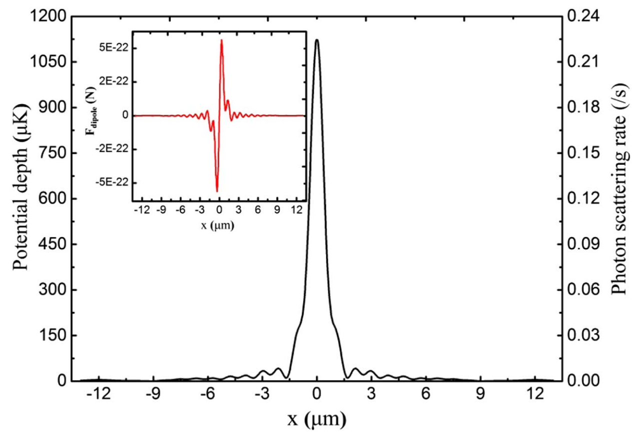

Fig. 4. Optical potential, dipole force, and scattering rate of optically trapped MgF molecules on the reflector with a focal length of 10 μm and a numerical aperture of 0.91 without missing grating strips. Inset: dipole force exerted on molecules in the laser field along the x direction.

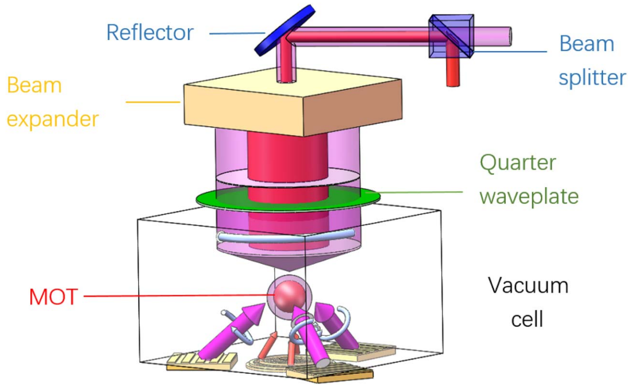

Fig. 5. Schematic of the grating MOT and the optical dipole trap of MgF molecules. Linearly polarized light (violet) at a wavelength of 359 nm and linearly polarized light (red) at a wavelength of 1550 nm are collimated by a beamsplitter, and circularly polarized light (gray arrows) by a quarter waveplate (green). An input beam of 359 nm is diffracted by three identical gratings on the periphery to create the MgF MOT (violet arrow indicates reflected MOT beams). An input beam of 1550 nm is reflected by the concentric grating in the center, resulting in a smaller trapping volume above the reflector (red arrow indicates reflected trapping beams).

than 1/s. When molecules are close to the surface of a reflector, some quantum effects, such as van der Waals potential, occur between the molecule and the grating. Actually, the van der Waals potential between them is very small, which is about 10^{-3} mK order of magnitude. So the Van der Waals potential has a low effect on trapped molecules.

Here, we propose a possible experimental setup to show the loading and trapping process of cold molecules in Fig. 5. First, an input beam of 359 nm is diffracted by three identical gratings on the periphery to form the MOT [23]. After that, we let the trapping light of 1550 nm be incident perpendicularly onto the designed circular grating reflector in the center, realizing the optical dipole well. In order to realize the molecule loading, the center of the potential well coincides with the central position of the MOT. Later, we turn off the 359 nm MOT laser and achieve optical dipole trapping for MgF molecules. We can also capture and manipulate viruses, bacteria, and individual cells in a solution with such a focused beam [36].

4. CONCLUSION

In summary, we have demonstrated the properties of the 2D concentric reflector in its structural parameters, numerical aperture, and fabrication-error-tolerant design. Our study shows that the grating reflector not only contains high reflectivity and a wide wavelength-tuning bandwidth but also exhibits high focusing ability. Under the incident polarized 1.55 μm illumination, the reflector can generate a focal spot with ~10 μm focal length and 0.85 μm linewidth. Missing grating strips in a certain range has minimal effect on the focusing performance of the reflector; the broad bandwidth characteristics allow the reflector to tolerate errors in fabrication. Such a focusing optical field on the metasurface reflector can provide the deep potential to trap the cold MgF molecules released from a standard MOT with a temperature of 532.7 μK; the maximum photon scattering rate in the optical trap is lower than 1/s. The optical trap with much smaller trap volumes and controllable trap depths can offer nearly state-independent potentials. This will allow for further laser cooling of trapped MgF molecules and lead to density enhancement for the small-scale volume on the order of the wavelength of the trapping light. It may be even feasible to achieve an optically trapped Bose–Einstein condensate of MgF molecules by optical-potential evaporative cooling [37].

Funding. National Natural Science Foundation of China (NSFC) (91836103, 11834003, 91536218, 11374100); Natural Science Foundation of Shanghai (17ZR1443000); 111 Project of China (B12024); Joint Research Institute for Science and Society.

REFERENCES

1. A. V. Kildishev, A. Boltasseva, and V. M. Shalaev, “Planar photonics with metasurfaces,” Science **339**, 1232009 (2013).
2. P. Genevet, F. Capasso, F. Aieta, M. Khorasaninejad, and R. Devlin, “Recent advances in planar optics: from plasmonic to dielectric metasurfaces,” Optica **4**, 139–152 (2017).
3. M. Khorasaninejad and F. Capasso, “Metalenses: versatile multifunctional photonic components,” Science **358**, eaam8100 (2017).
4. C. Pfeiffer and A. Grbic, “Metamaterial Huygens’ surfaces: tailoring wave fronts with reflectionless sheets,” Phys. Rev. Lett. **110**, 197401 (2013).
5. M. Decker, I. Staude, M. Falkner, J. Dominguez, D. N. Neshev, I. Brener, T. Pertsch, and Y. S. Kivshar, “High” efficiency dielectric Huygens’ surfaces,” Adv. Opt. Mater. **3**, 813–820 (2015).
6. Y. H. Fu, A. I. Kuznetsov, A. E. Miroshnichenko, Y. F. Yu, and B. Luk’yanchuk, “Directional visible light scattering by silicon nanoparticles,” Nat. Commun. **4**, 1527 (2013).
7. S. Person, M. Jain, Z. Lapin, J. J. Saenz, G. Wicks, and L. Novotny, “Demonstration of zero optical backscattering from single nanoparticles,” Nano Lett. **13**, 1806–1809 (2013).
8. L. Yin, V. K. Vlasko-Vlasov, J. Pearson, J. M. Hiller, J. Hua, U. Welp, D. E. Brown, and C. W. Kimball, “Subwavelength focusing and guiding of surface plasmons,” Nano Lett. **5**, 1399–1402 (2005).
9. Z. Liu, J. M. Steele, W. Srituravanich, Y. Pikus, C. Sun, and X. Zhang, “Focusing surface plasmons with a plasmonic lens,” Nano Lett. **5**, 1726–1729 (2005).
10. F. M. Huang, N. Zheludev, Y. Chen, and F. Javier Garcia de Abajo, “Focusing of light by a nanohole array,” Appl. Phys. Lett. **90**, 091119 (2007).
11. F. Monticone, N. M. Estakhri, and A. Alù, “Full control of nanoscale optical transmission with a composite metascreen,” Phys. Rev. Lett. **110**, 203903 (2013).
12. S. Jahani and Z. Jacob, “All-dielectric metamaterials,” Nat. Nanotechnology **11**, 23–36 (2016).
13. A. I. Kuznetsov, A. E. Miroshnichenko, M. L. Brongersma, Y. S. Kivshar, and B. Luk’yanchuk, “Optically resonant dielectric nanostructures,” Science **354**, aag2472 (2016).
14. D. Lin, P. Fan, E. Hasman, and M. L. Brongersma, “Dielectric gradient metasurface optical elements,” Science **345**, 298–302 (2014).
15. F. Lu, F. G. Sedgwick, V. Karagodsky, C. Chase, and C. J. Chang-Hasnain, “Planar high-numerical-aperture low-loss focusing reflectors and lenses using subwavelength high contrast gratings,” Opt. Express **18**, 12606–12614 (2010).
16. D. Fattal, J. Li, Z. Peng, M. Fiorentino, and R. G. Beausoleil, “Flat dielectric grating reflectors with focusing abilities,” Nat. Photonics **4**, 466–470 (2010).
17. A. Arbabi, Y. Horie, A. J. Ball, M. Bagheri, and A. Faraon, “Subwavelength- thick lenses with high numerical apertures and large

efficiency based on high-contrast transmitarrays," Nat. Commun. **6**, 7069 (2015).

18. X. F. Duan, G. R. Zhou, Y. Q. Huang, Y. F. Shang, and X. M. Ren, "Theoretical analysis and design guideline for focusing subwavelength gratings," Opt. Express **23**, 2639–2646 (2015).
19. H. Zhang, T. Li, Y. L. Yin, X. J. Li, Y. Xia, and J. P. Yin, "Microtrap on a concave grating reflector for atom trapping," Chin. Phys. B. **25**, 087802 (2016).
20. S. M. Wang, P. C. Wu, V. C. Su, Y. C. Lai, C. H. Chu, J. W. Chen, S. H. Lu, J. Chen, B. B. Xu, C. H. Kuan, T. Li, S. N. Zhu, and D. P. Tsai, "Broadband achromatic optical metasurface devices," Nat. Commun. **8**, 187 (2017).
21. S. M. Wang, P. C. Wu, V. C. Su, Y. C. Lai, M. K. Chen, H. Y. Kuo, B. H. Chen, Y. H. Chen, T. T. Huang, J. H. Wang, R. M. Lin, C. H. Kuan, T. Li, Z. L. Wang, S. N. Zhu, and D. P. Tsai, "A broadband achromatic metalens in the visible," Nat. Nanotechnol. **13**, 227–232 (2018).
22. O. Avayu, E. Almeida, Y. Prior, and T. Ellenbogen, "Composite functional metasurfaces for multispectral achromatic optics," Nat. Commun. **8**, 14992 (2017).
23. C. C. Nshii, M. Vangeleyn, J. P. Cotter, P. F. Griffin, E. A. Hinds, C. N. Ironside, P. See, A. G. Sinclair, E. Riis, and A. S. Arnold, "A surface-patterned chip as a strong source of ultracold atoms for quantum technologies," Nat. Nanotechnology **8**, 321–324 (2013).
24. J. P. McGilligan, P. F. Griffin, R. Elvin, S. J. Ingleby, E. Riis, and A. S. Arnold, "Grating chips for quantum technologies," Sci. Rep. **7**, 384 (2017).
25. E. Imhof, B. K. Stuhl, B. Kasch, B. Kroese, S. E. Olson, and M. B. Squires, "Two-dimensional grating magneto-optical trap," Phys. Rev. A **96**, 033636 (2017).
26. T. Shiono, M. Kitagawa, K. Setsune, and T. Mitsuyu, "Reflection micro-Fresnel lenses and their use in an integrated focus sensor," Appl. Opt. **28**, 3434–3442 (1989).
27. R. Grimm, M. Weidemuller, and Y. B. Ovchinnikov, "Optical dipole traps for neutral atoms," Adv. At. Mol. Opt. Phys. **42**, 95–170 (2000).
28. Y. N. Yin, S. P. Xu, T. Li, Y. L. Yin, Y. Xia, and J. P. Yin, "2D surface optical lattice formed by plasmon polaritons with application to nanometer-scale molecular deposition," Sci. Rep. **7**, 7788 (2017).
29. D. L. Gao, W. Q. Ding, M. N. Vesperinas, X. M. Ding, M. Rahman, T. H. Zhang, C. T. Lim, and C. W. Qiu, "Optical manipulation from the microscale to the nanoscale: fundamentals, advances, and prospects," Light: Sci. Appl. **6**, e17039 (2017).
30. T. H. Zhang, M. R. C. Mahdy, Y. M. Liu, J. H. Teng, C. T. Lim, Z. Wang, and C. W. Qiu, "All-optical chirality-sensitive sorting via reversible lateral forces in interference fields," ACS Nano **11**, 4292–4300 (2017).
31. M. M. Rahman, A. A. Sayem, M. R. C. Mahdy, M. E. Haque, R. Islam, S. T. Chowdhury, and M. A. Matin, "Tractor beam for fully immersed multiple objects: Long distance pulling, trapping, and rotation with a single optical set-up," Ann. Phys. **527**, 777–793 (2015).
32. C. W. Qiu, W. Q. Ding, M. R. C. Mahdy, D. L. Gao, T. H. Zhang, F. C. Cheong, A. Dogariu, Z. Wang, and C. T. Lim, "Photon momentum transfer in inhomogeneous dielectric mixtures and induced tractor beams," Light: Sci. Appl. **4**, e278 (2015).
33. M. R. Tarbutt, B. E. Sauer, J. J. Hudson, and E. A. Hinds, "Design for a fountain of YbF molecules to measure the electron's electric dipole moment," New J. Phys. **15**, 053034 (2013).
34. Y. N. Yin, Y. Xia, X. J. Li, X. X. Yang, S. P. Xu, and J. P. Yin, "Narrow-linewidth and stable-frequency light source for laser cooling of magnesium fluoride molecules," Appl. Phys. Express **8**, 092701 (2015).
35. X. X. Yang, C. L. Li, Y. N. Yin, S. P. Xu, X. J. Li, Y. Xia, and J. P. Yin, "Bichromatic slowing of MgF molecules in multilevel systems," J. Phys. B **50**, 015001 (2017).
36. A. Ashkin and J. M. Dziedzic, "Optical trapping and manipulation of viruses and bacteria," Science **235**, 1517–1520 (1987).
37. J. P. Yin, "Realization and research of optically-trapped quantum degenerate gases," Phys. Rep. **430**, 1–116 (2006).